Cell Reports

Article

Association of B cell profile and receptor repertoire with the progression of Alzheimer's disease

Graphical abstract

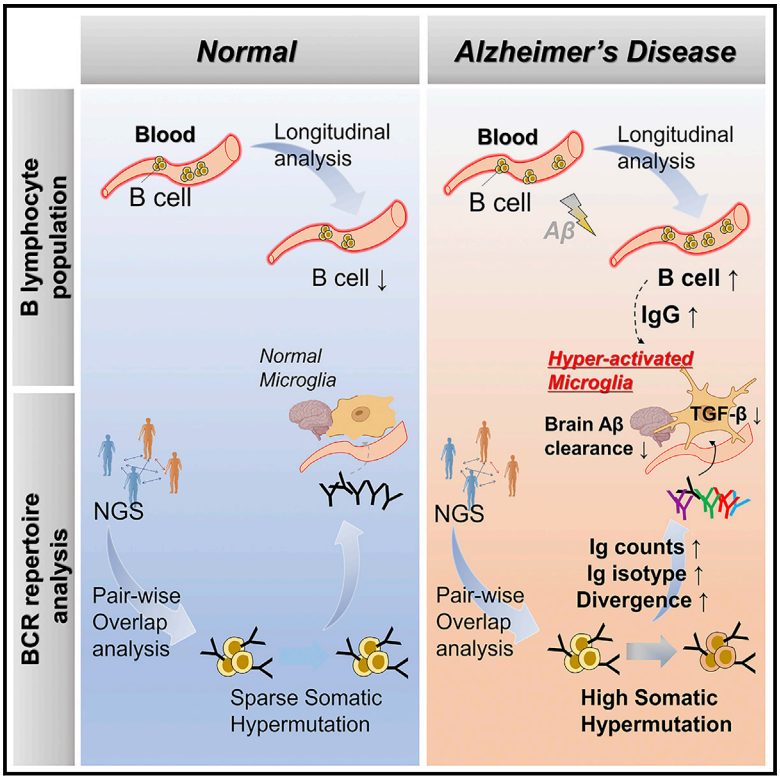

Highlights

- Longitudinal increase in B cells is associated with cerebral amyloid deposition
- B cell receptor repertoire profiling and pairwise sharing analysis are conducted
- Patients with Alzheimer's disease share similar class-switched BCR sequences
- B cell-derived immunoglobulin G induces microglial dysfunction in the brain

Authors

Jong-Chan Park, Jinsung Noh, Sukjin Jang, ..., Sun-Ho Han, Sunghoon Kwon, Inhee Mook-Jung

Correspondence

sunho@snu.ac.kr (S.-H.H.), skwon@snu.ac.kr (S.K.), inhee@snu.ac.kr (I.M.-J.)

In brief

Park et al. perform longitudinal analyses, B cell receptor repertoire profiling, and imaging analyses to identify the contribution of B lymphocytes to Alzheimer's disease pathology. They identify longitudinal increase in B lymphocyte populations, ensuing hyperactivation of microglia, and commonalities of BCR repertoires in Alzheimer's disease.

Park et al., 2022, Cell Reports *40*, 111391
September 20, 2022
https://doi.org/10.1016/j.celrep.2022.111391

CellPress

Cell Reports

CellPress
OPEN ACCESS

Article

Association of B cell profile and receptor repertoire with the progression of Alzheimer's disease

Jong-Chan Park,[1,2,3,4,17] Jinsung Noh,[5,13,17] Sukjin Jang,[6,17] Ki Hyun Kim,[7,8] Hayoung Choi,[1,3] Dongjoon Lee,[1,3] Jieun Kim,[1] Junho Chung,[7,8,9] Dong Young Lee,[10,11,12] Yonghee Lee,[5] Hyunho Lee,[5] Duck Kyun Yoo,[7,9] Amos Chungwon Lee,[13] Min Soo Byun,[11,12] Dahyun Yi,[12] Sun-Ho Han,[1,2,3,*] Sunghoon Kwon,[5,13,14,15,16,*] and Inhee Mook-Jung[1,2,3,18,*]

[1]Department of Biochemistry and Biomedical Sciences, College of Medicine, Seoul National University, Seoul 03080, Republic of Korea
[2]Neuroscience Research Institute, Medical Research Center, College of Medicine, Seoul National University, Seoul 03080, Republic of Korea
[3]SNU Dementia Research Center, College of Medicine, Seoul National University, Seoul 03080, Republic of Korea
[4]Department of Neurodegenerative Disease, UCL Queen Square Institute of Neurology, University College London, London WC1N 3BG, UK
[5]Department of Electrical and Computer Engineering, Seoul National University, 1 Gwanak-ro, Gwanak-gu, Seoul 08826, Republic of Korea
[6]Department of Medicine, Seoul National University College of Medicine, Seoul 03080, Republic of Korea
[7]Department of Biochemistry and Molecular Biology, Seoul National University College of Medicine, 103 Daehak-ro, Jongno-gu, Seoul 03080, Republic of Korea
[8]Cancer Research Institute, Seoul National University College of Medicine, Seoul 03080, Republic of Korea
[9]Department of Biomedical Science, Seoul National University College of Medicine, Seoul 03080, Republic of Korea
[10]Institute of Human Behavioral Medicine, Medical Research Center, Seoul National University, Seoul 03080, Republic of Korea
[11]Department of Psychiatry, College of Medicine, Seoul National University, Seoul 03080, Republic of Korea
[12]Department of Neuropsychiatry, Seoul National University Hospital, Seoul 03080, Republic of Korea
[13]Bio-MAX Institute, Seoul National University, Seoul 08826, Republic of Korea
[14]BK21+ Creative Research Engineer Development for IT, Seoul National University, Seoul 08826, Republic of Korea
[15]Biomedical Research Institute, Seoul National University Hospital, Seoul 03080, Republic of Korea
[16]Interdisciplinary Program in Bioengineering, Seoul National University, Seoul 08826, Republic of Korea
[17]These authors contributed equally
[18]Lead contact
*Correspondence: sunho@snu.ac.kr (S.-H.H.), skwon@snu.ac.kr (S.K.), inhee@snu.ac.kr (I.M.-J.)
https://doi.org/10.1016/j.celrep.2022.111391

SUMMARY

Alzheimer's disease (AD) is the most prevalent type of dementia. Reports have revealed that the peripheral immune system is linked to neuropathology; however, little is known about the contribution of B lymphocytes in AD. For this longitudinal study, 133 participants are included at baseline and second-year follow-up. Also, we analyze B cell receptor (BCR) repertoire data generated from a public dataset of three normal and 10 AD samples and perform BCR repertoire profiling and pairwise sharing analysis. As a result, longitudinal increase in B lymphocytes is associated with increased cerebral amyloid deposition and hyperactivates induced pluripotent stem cell-derived microglia with loss-of-function for beta-amyloid clearance. Patients with AD share similar class-switched BCR sequences with identical isotypes, despite the high somatic hypermutation rate. Thus, BCR repertoire profiling can lead to the development of individualized immune-based therapeutics and treatment. We provide evidence of both quantitative and qualitative changes in B lymphocytes during AD pathogenesis.

INTRODUCTION

Recent studies have shown that Alzheimer's disease (AD) phenotypes are not limited to brain changes. There is increasing evidence that the peripheral immune system is closely linked to AD pathology, especially the critical role of immune cells in the pathogenesis of AD (Goldeck et al., 2016; Park et al., 2020). To date, however, there has been little discussion regarding the contribution of blood lymphocytes in AD. Several studies have revealed the possible association between blood lymphocytes and the decline in cognitive function or accumulation of cerebral amyloid deposition in AD. These studies have been conducted as cross-sectional studies using lymphocyte population data or failed to correlate specific lymphocyte characteristics with the pathology of AD (Cao and Zheng, 2018; Poinsatte et al., 2019; Richartz-Salzburger et al., 2007). Although recent technologies, such as B cell receptor (BCR) or T cell receptor (TCR) next-generation sequencing (NGS)-based repertoire profiling have been developed

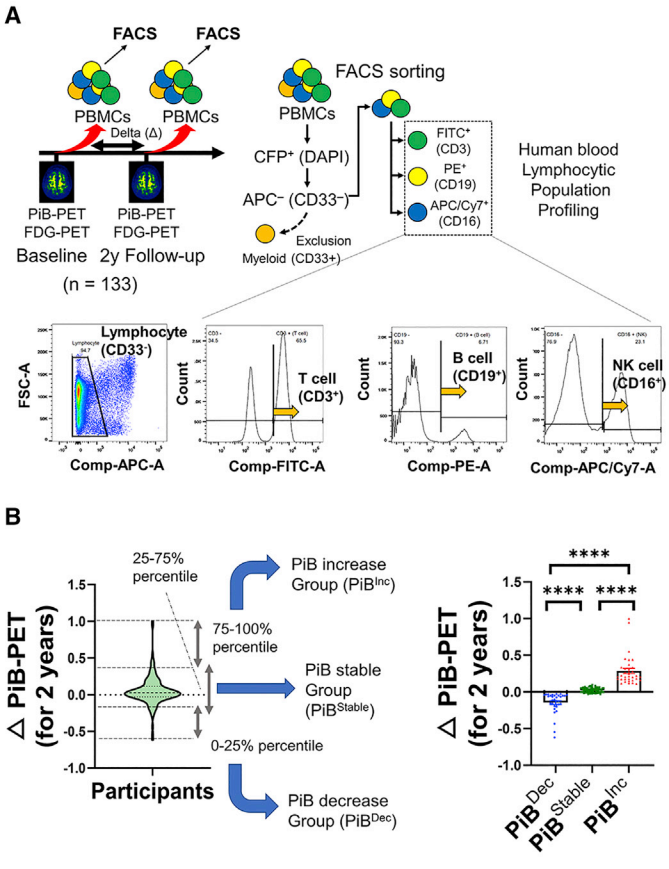

C

Multiple regression analysis

Dependent variable: Δ Global PiB deposition (SUVR)						Method: Stepwise
Indep. variable	β	SE	t	*P* value	F-ratio (DF)	Adj-R^2
Δ B cell	0.0065	0.0017	3.698	**0.0003*** **	13.67 (1, 131)	0.088
Excluded variables: Δ NK cell, Δ T cell, Age, Gender						

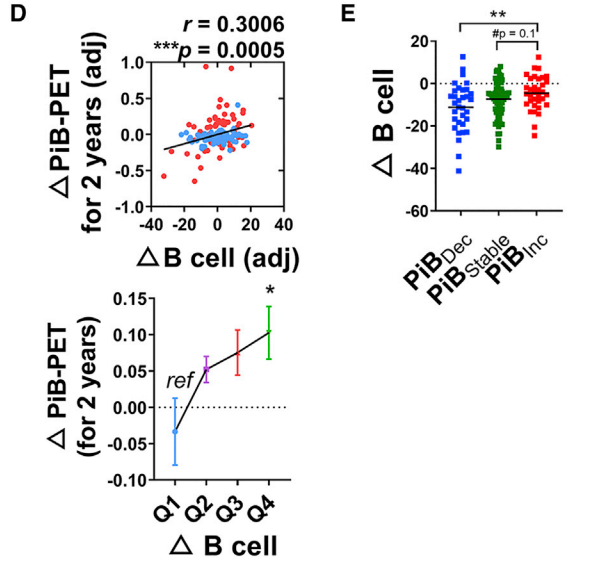

Figure 1. Strategy for longitudinal analysis

(A and B) Timeline of the longitudinal study (n = 133). Brain imaging and isolation of peripheral mononuclear cell (PBMC) were performed at both baseline (BL) and second-year follow-up (FL) time point. Classification of the PBMCs by the FACS analysis ($CD3^+$ for T lymphocytes, $CD19^+$ for B lymphocytes, and $CD16^+$ for NK lymphocytes). Participants were classified into three groups for the in-depth analyses (PiB increase group, PiB^{Inc}, getting worse for 2 years; PiB stable group, PiB^{Stable}, none the worse for 2 years; PiB possible decrease group, PiB^{Dec}, relatively getting better for 2 years). Error bar, standard error of mean.

(C) Stepwise multiple regression analysis between the change in (Δ) lymphocytes (B, T, NK lymphocytes) and Δ global PiB deposition (standardized uptake value ratio; SUVR). Age and gender were also included as covariates. Only B lymphocyte is selected by the stepwise method.

(D) Partial correlation analysis between Δ global PiB SUVR and ΔB lymphocytes (***$p < 0.001$, left) and ANOVA with post-hoc test between the quartiles of ΔB lymphocytes (Q1 < Q2 < Q3 < Q4) and Δ global PiB SUVR. Error bar, standard error of mean.

(E) PiB^{Inc} group significantly showed less decrease in B cell population than those of the PiB^{Dec} group for 2 years (**$p < 0.01$, ANOVA with Tukey's post-hoc test). Error bar, standard error of mean.

(Bashford-Rogers et al., 2019; Davis et al., 2019; Soto et al., 2019), few studies have applied these tools to the study of AD (Gate et al., 2020). In particular, no study exists on BCR repertoire analysis in AD. Therefore, this study aimed to identify the type of lymphocytes that are directly linked to brain amyloid deposition and to discover the characteristics of BCR repertoires shared among patients with AD. We found that an increase in the population of B lymphocytes over 2 years and immunoglobulin G (IgG) during the progression of AD was significantly associated with an increase in cerebral β-amyloid (Aβ) deposition. Furthermore, BCR sequencing, followed by pairwise sharing analysis revealed the commonalities of BCR repertoires within patients with AD, but not within normal participants. This approach, through both longitudinal analysis and BCR repertoire profiling, provides a perspective for understanding the link between the peripheral immune system and neuropathology in the brains of patients with AD.

RESULTS

The longitudinal study revealed that B lymphocyte population is associated with brain amyloid deposition in AD

Figure 1A shows the overall strategy for flow cytometry analysis (Figure S1), followed by a longitudinal analysis of B lymphocyte population changes. A total of 133 participants that underwent Pittsburgh compound B-positron emission tomography (PiB-PET) scans to image Aβ plaques in their brains were included in this study. For longitudinal analyses, we assigned the participants into three groups: PiB decrease group (PiB^{Dec}; a group with disease mitigation), PiB stable group (PiB^{Stable}; a group without progression of AD pathology), and PiB increase group (PiB^{Inc}; a group with progression of AD pathology), based on the changes in PiB-PET standardized uptake value ratio (SUVR) after 2 years

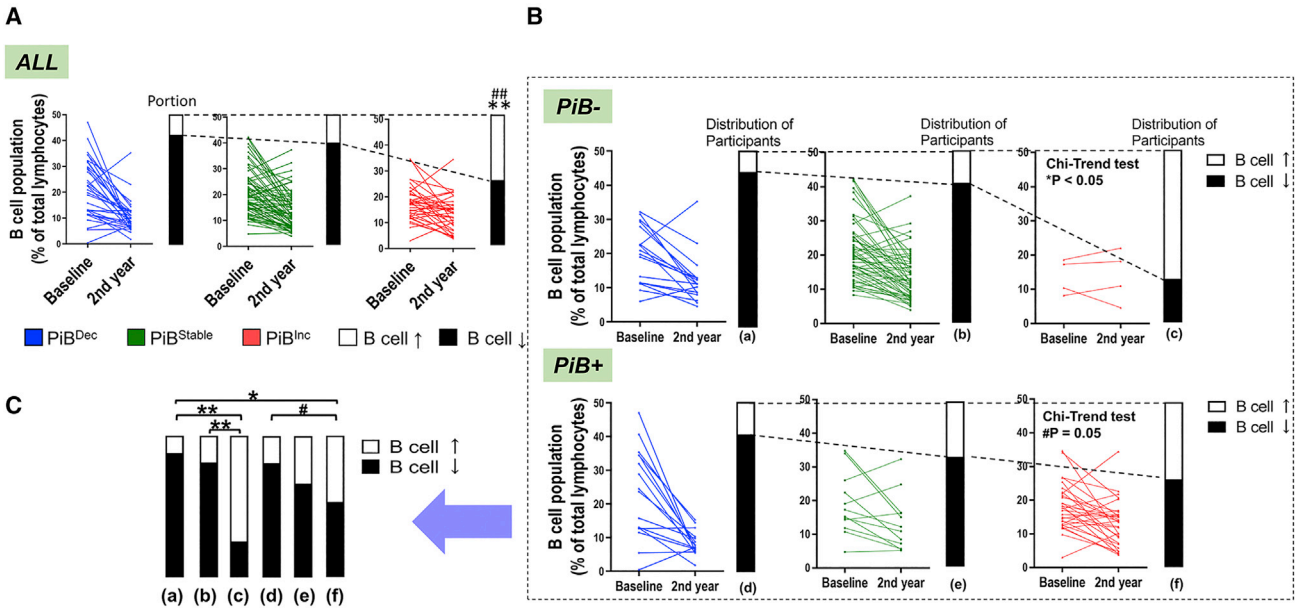

Figure 2. The increase in B cell in PiB^{Inc} group

(A) B lymphocyte changes between baseline and follow-up second year. PiB^{Inc} group has higher portion of B cell-increased participants than those of the PiB^{Dec} and PiB^{Stable} groups (Chi-trend test, $^{\#\#}p < 0.01$; Chi-squared test, $^{**}p < 0.01$).

(B) PiB^{Inc} group has a higher portion of B cell-increased participants than those of the PiB^{Dec} and PiB^{Stable} group both in PiB− and PiB+ (Chi-trend test, $^{\#}p < 0.10$, $^{*}p < 0.05$).

(C) Chi-squared test ($^{\#}p < 0.10$, $^{*}p < 0.05$, $^{**}p < 0.01$).

(Figure 1B and Table S1). Stepwise multiple regression analysis showed that the population change in B lymphocytes over 2 years (ΔB) was significantly associated with an increase in brain Aβ (change in PiB SUVR; ΔPiB), but the changes in other lymphocytes (ΔT cells, ΔNK cells) were not (Figure 1C). In addition, only ΔB showed a significant correlation with ΔPiB in the cognitively normal (CN) population, indicating a direct association between B cells and brain Aβ (Figure S2). This was the decisive reason to focus on the profiling of B cells. We also confirmed that the number of B cells decreased with age, as previously reported (Frasca and Blomberg, 2011, 2020), but we did not observe a significant decrease in the dementia group (Figure S3). Next, partial correlation and ANOVA post-hoc analysis showed that ΔB was positively correlated with ΔPiB (Figure 1D, upper graph), and ΔB quartile four (Q4) had the highest ΔPiB value (Q1 < Q2 < Q3 < Q4; Figure 1D, lower graph). Moreover, PiB^{Inc} had a higher ΔB than PiB^{Dec} and PiB^{Stable} (Figure 1E). Furthermore, comparative analyses between the three groups PiB^{Dec}, PiB^{Stable}, and PiB^{Inc} were performed. Interestingly, PiB^{Inc} had a higher proportion of participants with an increasing number of B lymphocytes (Figure 2A), regardless of the baseline status of Aβ accumulation (Figures 2B and 2C). For the logistic regression analysis, the independent variables were age, sex, and ApoE with or without ΔB, and the dependent variables were PiB^{Dec} + PiB^{Stable} (control) versus PiB^{Inc} (case). The receiver operating characteristic curve analysis showed that ΔB increased the discrimination power of PiB^{Inc} as an independent variable in the logistic regression analysis (Figure 3A). The combination of ApoE and ΔB variables had higher sensitivity (70.6%) and specificity (72.7%) with a 0.754 area under the curve (AUC) than ApoE alone (0.710 AUC with 55.9% sensitivity and 76.8% specificity) (Figure 3B). We also performed precision-recall curve - analysis and comparison analysis with the bootstrap method to reduce imbalance bias in the two classes and obtained significant results (Figures 3C and 3D). For further validation, we classified participants according to their ΔB quartiles (BQ; BQ1 < BQ2 < BQ3 < BQ4) and compared their ΔPiB. The BQ4 and BQ2–3 groups had higher ΔPiB values than that of BQ1 (Figure 3E), and these results led us to focus on B lymphocyte profiling in subsequent studies.

RNA sequencing analysis implied qualitative B cell differences between CN and AD

Before deep profiling of B lymphocytes, we performed RNA sequencing analysis using a public cohort (GEO: GSE18309), including transcriptome data from human peripheral blood mononuclear cell (PBMC) samples (elderly normal controls, n = 3; AD patients, n = 3; Taiwanese) (Figure 4). We detected 1,478 downregulated genes and 1,031 upregulated genes from the dataset ($p < 0.05$; significance by limma in R by GEO2R analyzer) (Figure 4A) and selected B cell-related genes that overlapped with the Gene Ontology (GO) database. Interestingly, 11 genes from the B cell-mediated immunity term (GO: 0019724) overlapped and were significantly different between the normal and AD groups (Figure 4B). In addition, although SLAMF8 (B cell activator) decreased in AD and the B cell homeostatic proliferation gene (GO: 0002358) and FOXP3 expression were significantly decreased in AD, the B cell differentiation/positive regulation genes (RAG2, IL-10; GO: 0002335 and 0002327) were

A

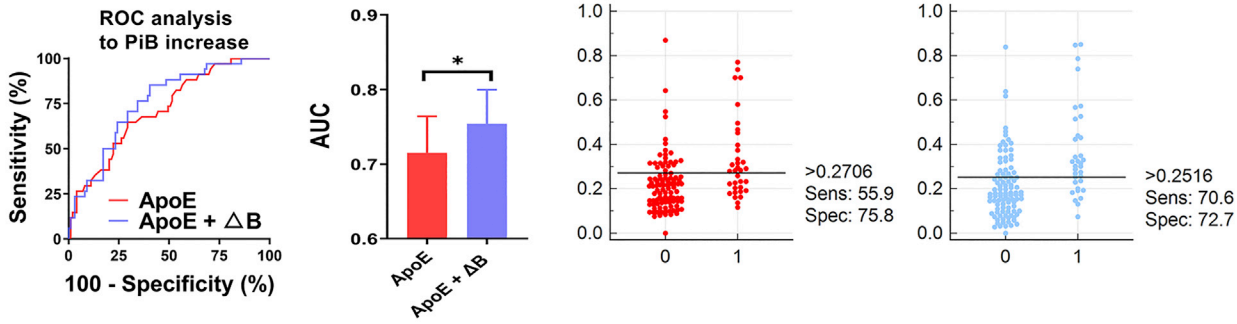

B

ROC curve analysis for PiB-PET increase using B lymhocytes				
Variables	**AUC**	**SE**	**95% CI**	**Sensitivity/Specificity (%)**
ApoE	0.710	0.0493	0.614 to 0.807	55.88/75.77
ApoE + ΔB	0.757	0.0458	0.668 to 0.847	70.59/72.73

Comparison of ROC curve analysis for PiB-PET increase				
Control model	**Improved model**	**Continuous NRI**	**SE**	***P* value (NRI)**
ApoE	ApoE + ΔB	0.4272	0.1988	*0.0316

E

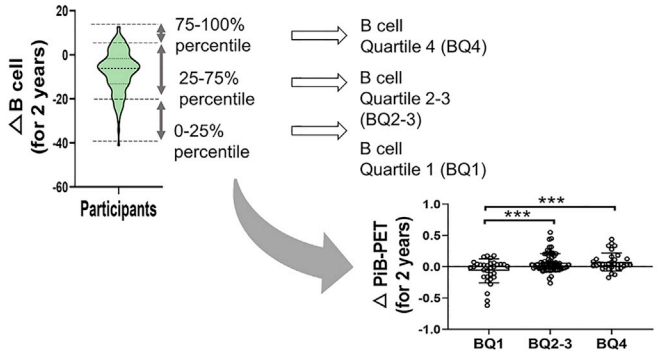

C

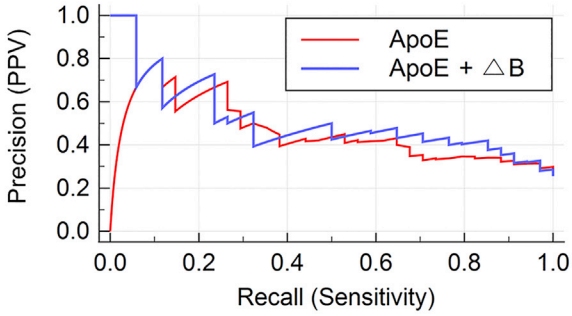

D

Precision-Recall curve for PiB-PET increase using B lymphocytes				
Variables	**AUC**	**95% CI**	**$F1_{max}$**	**Associated criterion**
ApoE	0.454	0.297 to 0.620	0.518	> 0.2584
ApoE + ΔB	0.509	0.346 to 0.670	0.563	> 0.2035

Comparison of Precision-Recall curve analysis for PiB-PET increase				
Control model	**Improved model**	**Difference between areas**	**95% Bootstrap CI**	**Significance**
ApoE	ApoE + ΔB	0.0548	0.0189 to 0.1174	*P* < 0.05 (Yes)

(1000 iterations; random number seed: 978).

Figure 3. Longitudinal analysis and receiver operation characteristic curve (ROC) analysis for B lymphocyte profiling

(A and B) B cell biomarkers showed better discrimination power to PiB progression when combined with ApoE genotyping. *p < 0.05 by continuous net reclassification index (NRI). Interactive dot diagram showed sensitivity/specificity/cutoff (p_i values by Youden index, > 0.2706, >0.2516) values for PiB increase ROC curves. For logistic regression analysis, independent variables were age, sex, and ApoE with or without ΔB, and dependent variables were PiB^{Dec} + PiB^{Stable} (control) versus PiB^{Inc} (case). Error bar, standard error of mean.

(C and D) Precision-recall curve analysis and comparison of analysis with the bootstrap method to reduce imbalance bias between the two classes.

(E) Participants were re-classified according to their quartiles of ΔB lymphocytes (BQ1 < BQ2 < BQ3 < BQ4) and divided into three groups (BQ1, BQ2–3, BQ4). ΔPiB-PET values were significantly increased in BQ2–3 and BQ4 compared with BQ1 (***p < 0.001; ANOVA with Tukey's post-hoc test). Two outliers were excluded by Grubb's test.

significantly increased in AD (Figure 4C). Moreover, B cell lineage commitment genes (GO: 0002326), isotype switching genes (GO: 00045190), and immunoglobulin complex circulating genes (GO: 0042571) were different between the normal and AD groups (Figure 4C). In particular, previous reports have shown that (1) overexpression of FOXP3 induces a reduction in antibody response or diminished B cell antibody production (Kasprowicz et al., 2003), (2) the absence of RIF1 increases the number of B cells with IgG2/IgM (Di Virgilio et al., 2013), and (3) the role of PIGR is related to the production of secretory IgA (Lycke and Bemark, 2017), which implies qualitative B cell differences between normal individuals and patients with AD.

Pair-wised sharing analysis followed by NGS-based BCR repertoire analysis

For deep profiling of B lymphocytes at the BCR sequence level, we randomly selected 13 representative participants (three normal, 10 AD) with an even distribution of ApoE allele frequencies (two ϵ3/ϵ3

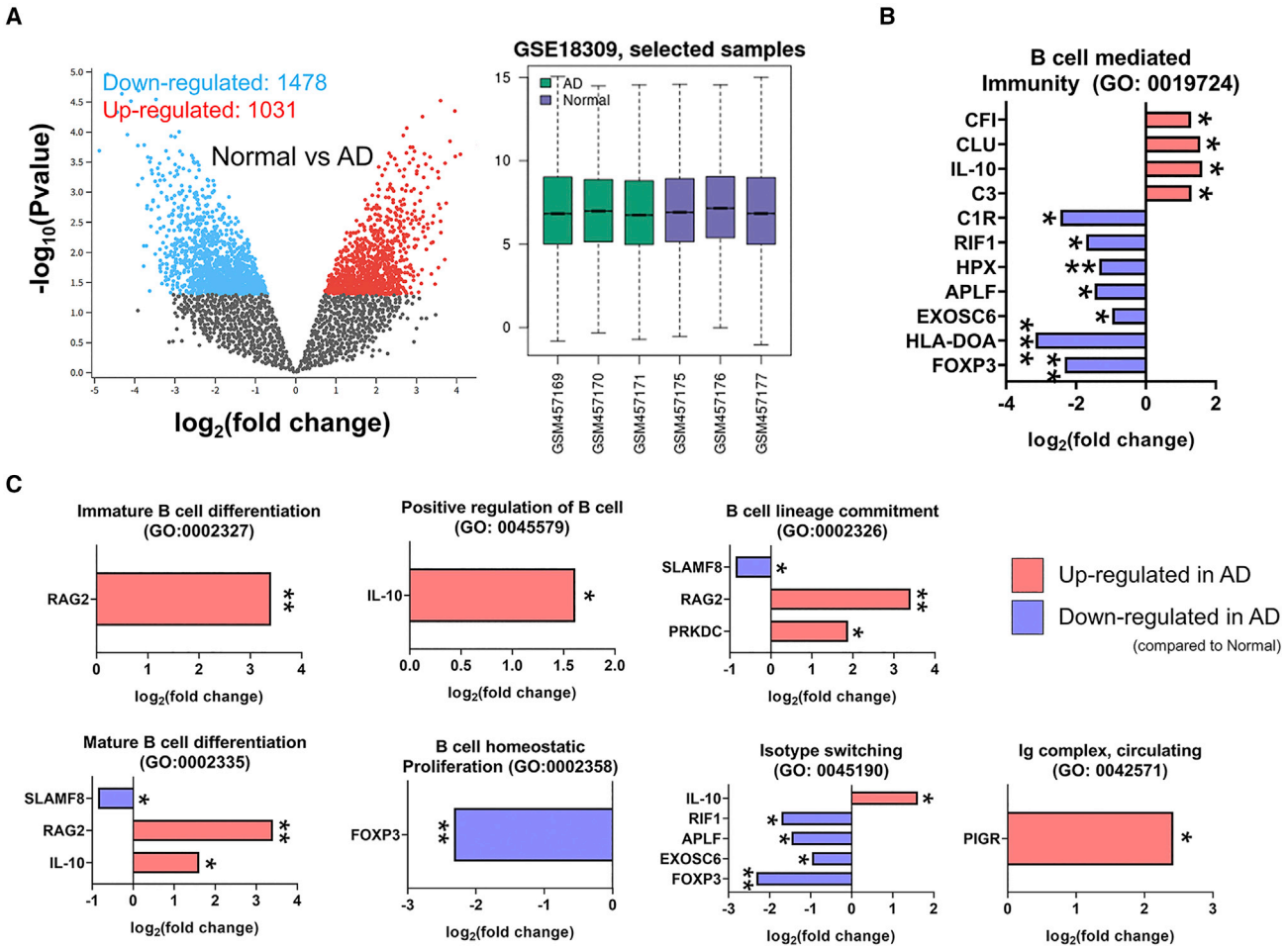

Figure 4. RNA sequencing analysis using a dataset from public Gene Expression Omnibus database (GEO: GSE18309)

(A) Volcano plot and distribution plot for the dataset (n = 3 elderly normal controls versus n = 3 AD; human PBMC samples).

(B) Significant genes associated with Gene Ontology database (term: B cell mediated immunity; GO: 0019724). *p < 0.05, **p < 0.01, and ***p < 0.001 with log-transformation to the data.

(C) Significant genes associated various B cell-related terms (GO: 0002327, 0045579, 0002326, 0002335, 0002358, 0045190, and 0042571). *p < 0.05 and **p < 0.01 with log-transformation to the data. For the analysis, GEO2R analyzer was used.

and one ϵ3/ϵ4 for normal; three ϵ3/ϵ3, four ϵ3/ϵ4, three ϵ4/ϵ4 for AD), ages (73.6 ± 1.9 for normal, 68.6 ± 2.2 for AD), and the number of total lymphocytes (30.7 ± 3.4 for normal, 31.6 ± 2.6 for AD) that can interfere with the analysis of B lymphocytes (Allan et al., 2009; Frasca and Blomberg, 2009; Richartz-Salzburger et al., 2007) (Figure 5A). The cerebral amyloid deposition (SUVR), Mini-Mental State Examination (MMSE) cognitive score, plasma t-tau, and Aβ 42/40 ratio were significantly different between the normal and AD groups, but the age was not (Figures 5B and 5C). We generated BCR repertoire data from the normal and AD samples and annotated them as Normal (n = 3; "Normal 1") and AD (n = 10), respectively. In addition, to compensate for the limited number of healthy controls, we generated BCR repertoire data from an additional 52 recruited healthy individuals using the same protocol, except for the NGS platform (see STAR Methods). The additional healthy control data were annotated as Normal 2. We annotated the data of the two healthy controls with different names and focused our analysis on the comparison between AD and Normal because the age distributions of Normal and Normal 2 were significantly different and AD-related metrics were not available for Normal 2 (Figure S4).

At the whole BCR repertoire level, we investigated variable (V) gene usage of the samples. We did not detect a significant difference in V gene usage between the AD and normal groups after p value correction for multiple comparisons. We found that the previously reported V gene usage was reproduced in the two groups (Figure S5). We then investigated the differences in clonal characteristics through clonal expansion and clonal diversification indices (Bashford-Rogers et al., 2019). For the clonal expansion index, AD showed significantly lower values than the normal group. In addition, AD showed lower (but not significant) clonal diversification index values than the normal group (Figure S6). These results indicate that more oligo-clonal patterns exist in the Normal compared with that in the AD groups. Collectively, the increased B cell population in AD can be interpreted as the result of the

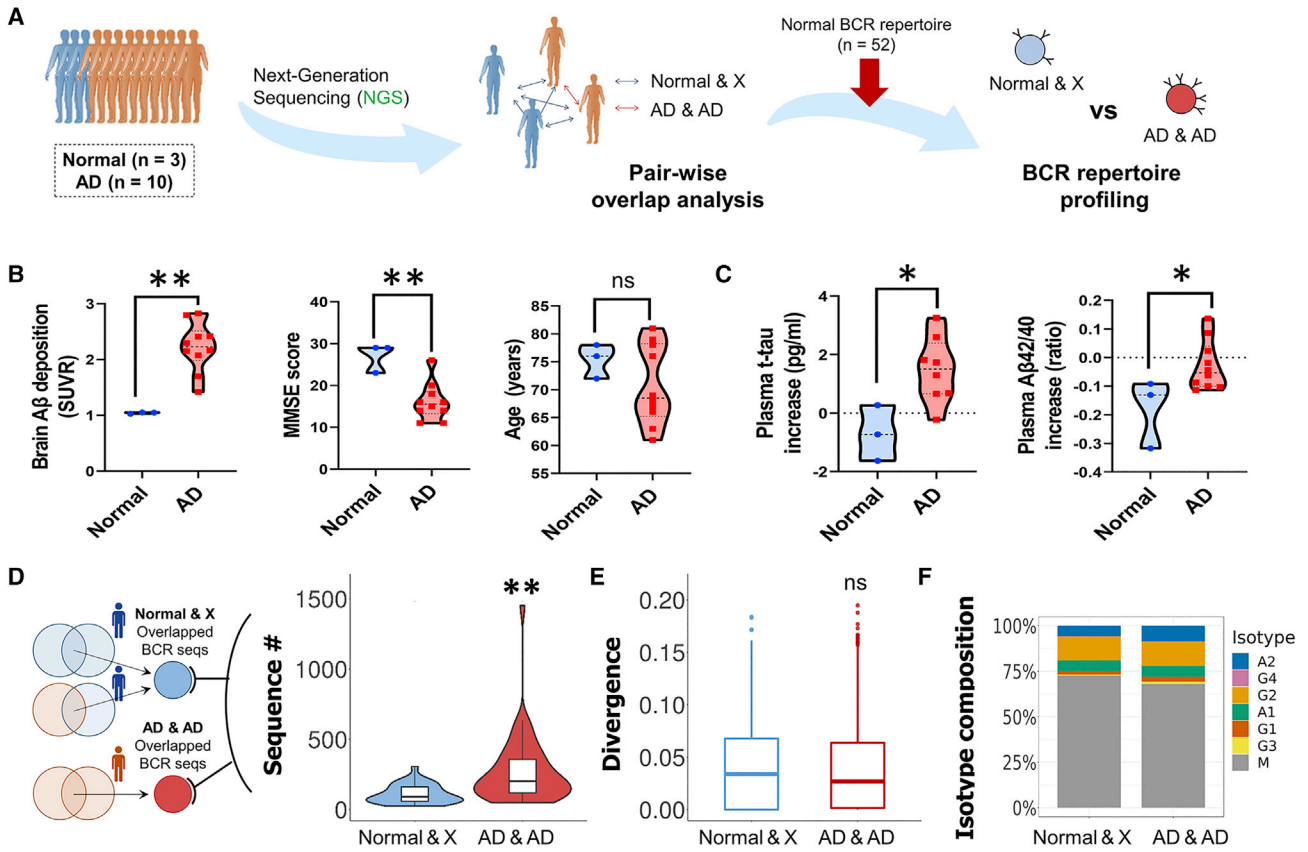

Figure 5. NGS-based BCR repertoire profiling followed by pairwise BCR sharing analysis

(A) B cell receptor (BCR) repertoire analysis (n = 13). A total of 13 participants (10 AD patients and three cognitively normal controls) were used for the BCR repertoire analysis. Shared BCR sequences were defined by pairwise sharing analysis of the BCR repertoire of the samples, which was followed by comparative analysis between Normal&X (comparison between Normal and Normal or Normal and AD; blue bidirectional arrow of the upper panel) and AD&AD (comparison between AD and AD; red bidirectional arrow of the upper panel) groups.

(B) Characterization of samples subjected to BCR repertoire analysis. *$p < 0.05$ and **$p < 0.01$, independent t test.

(C) The changes in the levels of plasma t-tau and beta-amyloid 42/40 ratio. *$p < 0.05$, independent t test.

(D) The number of shared BCR sequences resulted from pairwise sharing analysis. AD&AD had more shared BCR sequences than that of Normal&X. **$p < 0.001$; Wilcoxon rank-sum test.

(E) Divergence of the shared BCR sequences.

(F) Isotype composition of the shared BCR sequences.

expansion of clonally unrelated B cells. However, the clonal expansion and diversification indices of AD and Normal tissues were significantly higher than previously reported values. Aging affects the BCR repertoire, especially clonal characteristics (de Bourcy et al., 2017). In addition, the Normal 2 group of younger patients showed comparable clonal expansion and diversification index values to those previously reported. Based on these results, we concluded that the discrepancy in clonal indices between the AD and Normal groups was due to the high age distribution of the groups. In other whole BCR characteristics, such as isotype distribution, joining (J) gene usage, and somatic hypermutation (SHM) patterns, we did not observe significant differences between the groups (Figures S7–S9).

To discover the BCR characteristics of the AD samples, we focused our analysis on a subset of the entire BCR repertoire shared among the patients. Briney et al. investigated the sharing of BCR repertoires between multiple individuals through leukapheresis, followed by NGS with extremely high sequencing depth (Briney et al., 2019). In this study, it was shown that approximately 1% of BCRs were shared between two individuals, and 0.022% of BCRs were shared among 10 individuals. However, in this study, we applied a sampling strategy with a limited throughput (10 mL of blood and $\sim 10^5$ sequencing reads after preprocessing). Thus, we expected that few BCRs would be shared among multiple individuals with AD and normal individuals. In the preliminary sharing analysis, we found that only three clonotypes were exclusively shared between more than two patients with AD.

Considering previous research and our shallow sampling depth, we decided to conduct a pairwise analysis to define shared BCRs. We defined shared BCRs using AD and normal datasets that were derived from age-matched samples and tagged with AD-related measurements. The Normal 2 dataset was used to exclude universal BCRs that were also detected in the healthy population. Shared BCR sequences were categorized into two groups, Normal&X

(comparison between normal and normal or normal and AD) and AD&AD (comparison between AD and AD) (Figures 5A and 5D left), according to the sharing pattern. We hypothesized that sharing between Normal and AD has an identical pattern to that between Normal and Normal, because the two groups of samples do not share common immunological stimuli. Thus, we defined the two comparisons collectively as Normal&X and compared them with AD&AD. Interestingly, AD&AD had more shared BCR sequences and lineages than Normal&X (Figure 5D, right). The number of shared BCRs is vulnerable to the sequencing depth and clonal diversity. After sub-sampling of the raw data and normalization using the entire number of BCRs, a high representation of shared BCRs in AD&AD was reproduced. In addition, the Normal&Normal and Normal&AD groups showed no significant differences in sharing patterns, justifying our approach to defining them as Normal&X collectively (Figure S10). However, in terms of divergence and isotype composition, the two groups showed no significant differences (Figures 5E and 5F).

Pairwise sharing analysis with highly similar shared BCR sequences revealed the commonalities of its repertoires in patients with AD

To exclude coincidently defined shared BCR sequences and investigate shared BCR sequences in a stricter manner, we calculated the inter-sample variable-region full amino acid (AA) distance (shorter distance indicates higher similarity) of the shared BCR sequences (Setliff et al., 2018). We defined the shared BCR sequences by VJ gene usage (related to the mechanism of somatic recombination) (Roth, 2014) and complementarity-determining region 3 (CDR3; the most variable portion of Ig molecules) (VanDyk and Meek, 1992) AA sequence homology (>70%) as previously reported (Ehrhardt et al., 2019; Setliff et al., 2018). In addition, owing to the limited resolution of the criteria used, BCR sequences with distinctive SHM patterns (a process diversifying BCRs through point mutations into Ig genes) (Cui et al., 2016) were included in the shared BCR sequences. Thus, we quantified the degree of SHM sharing by defining the inter-sample variable-region full AA distance as the Hamming distance calculated at the variable-region full AA level between the shared BCR sequences from the different samples (Gupta et al., 2017). AD&AD showed a shorter inter-sample variable-region full AA distance compared with that of Normal&X (Figure 6A, left). The sub-population of the shared BCR sequences with a small inter-sample variable-region full AA distance (<5) was extracted and defined as highly similar shared BCR sequences. The highly similar shared BCR sequences can be generated in two ways. First, for naive B lymphocytes, gene rearrangement could generate coincidentally similar CDR3 with some bias inherent in the process. These sequences would have a very small number of SHMs and are in the IgM or IgD isotype (Briney et al., 2019; Soto et al., 2019). Second, for activated B lymphocytes, the induction of somatic mutations by antigens can produce converged BCR sequences (Jackson et al., 2014; Parameswaran et al., 2013). In this case, the sequences had high divergence values and were class-switched to isotypes other than IgM and IgD. These highly similar shared BCR sequences of AD&AD showed distinctive characteristics with respect to divergence and isotype composition compared with those of Normal&X. Among the sequences, sequences with a high divergence despite a small inter-sample variable-region full AA distance were only detected in AD&AD, indicating that mutation induction in the same direction resulted in identical residues for binding that occurred only in AD&AD (Figure 6A, right). In addition, Ig counts were significantly increased in AD&AD group (Figure 6B). Although AD&AD and Normal&X showed significantly different shared Ig count values, these Ig count values were vulnerable to sequencing depth and clonal diversity of the repertoires. In addition, this high sharing between the AD samples could be derived from a random effect. To calculate the statistical significance of the observed Ig count values, we conducted a randomized sharing simulation using the throughput-adjusted Normal 2 data and compared our Ig count values with the simulation results, which resulted in a significant p value of 0.0136 (Tables S3 and S4 and Figure S11). Furthermore, most of the sequences with high divergence values were class-switched to isotypes other than IgM (Figure 6C). A total of 579 sequences and 108 lineages were class-switched among highly similar shared BCR sequences. Among 108 lineages, 92 contained more than one class-switched BCR sequence in both repertoires with a distinctive VJ gene utilization compared with the whole class-switched repertoires of the samples (Figure 6D and Tables S3 and S5 and Figure S12). Strikingly, in 91 out of 92 lineages, BCR sequences were represented by identical isotypes in two different repertoires, indicating that it is feasible for these sequences to result in the same effector functions. In one lineage with different isotypes, the sequences emerged as IgA1 and IgA2 (Figure 6E). These identical characteristics of the highly similar and class-switched shared sequences were also reproduced in hierarchical clustering analysis by confirming that the sequences from different samples were clustered into the same subfamily with identical isotypes (Figure S13). We conclude that there is a possible response to stimulation by the same antigen (Park et al., 2017, 2019). In other words, the commonalities of the BCR repertoires in patients with AD imply the possibility of immunological stimuli by common antigens.

The increase in IgG can lead to the loss-of-function of microglia and dysregulation of Aβ clearance

Since we confirmed that the association of B cells increases with the progression of AD and there are significant differences in Ig counts between normal and AD patients, we further assessed the contribution of this phenomenon to the brain. We hypothesized that more IgGs will be produced by the increase in B cells and can cross the blood-brain barrier, as previously reported (David Morgan et al., 2016; Kim et al., 2021; Struemper et al., 2022; Villasenor et al., 2016). Thus, we treated human induced pluripotent stem cell (iPSC)-derived microglia with IgG, both in mild Aβ (acute model) and severe Aβ conditions (chronic model), similar to our previous report (Baik et al., 2019) (Figures 7A and 7B). Interestingly, microglia showed enhanced phagocytic activity following IgG treatment in the acute model, although no changes were observed in transforming growth factor β (TGF-β) levels or in Aβ plaque intensity (Figure 7C). However, in the

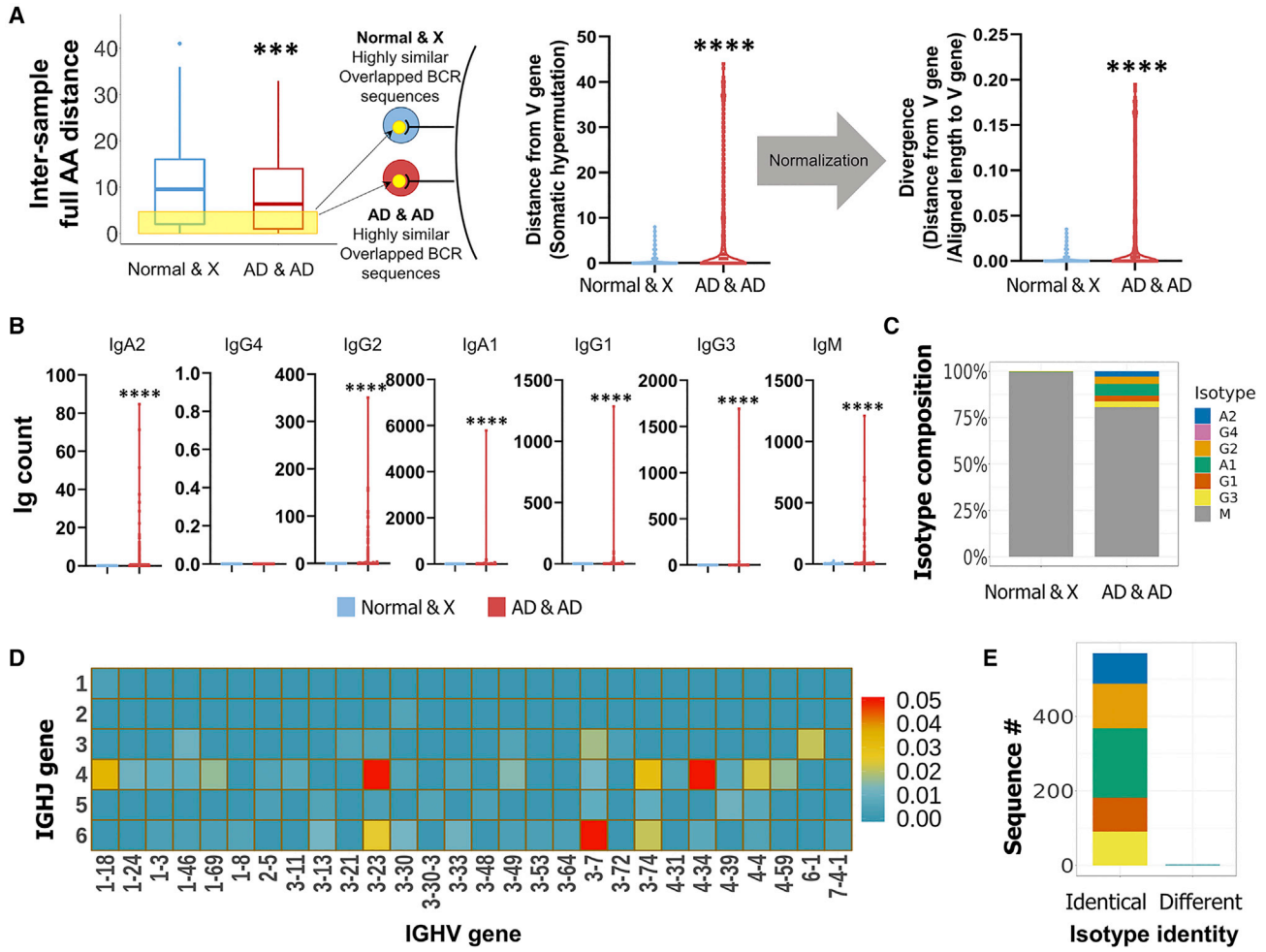

Figure 6. NGS-based BCR repertoire profiling followed by pairwise BCR sharing analysis (high similar shared sequences)

(A) Inter-sample full amino acid (AA) distance of the shared BCR sequences. The averaged Hamming distance between BCR sequences, which were shared and derived from different samples, was calculated using full AA sequences. This distance was named as inter-sample full AA distance. Among the shared BCR sequences, sequences with inter-sample full AA distance value smaller than 5 were defined as "highly similar shared BCR sequence." Significantly increased divergence of highly similar shared BCR sequences in the AD&AD group. ****$p < 0.0001$; Wilcoxon rank-sum test.

(B) The number of Ig counts between Normal&X versus AD&AD. ****$p < 0.0001$; Mann-Whitney test.

(C) Isotype composition of the highly similar shared BCR sequences. Despite a small inter-sample full AA distance, the sequences with a high divergence were only shown in AD&AD.

(D) VJ gene usage of the class-switched and highly similar shared BCR sequences.

(E) Isotype identity of the class-switched and highly similar shared BCR sequences. Matches in isotypes in different samples of the class-switched and highly similar shared BCR sequences were quantified. If the isotypes of sequences were identical in different two samples, they were counted as "identical." If not, they were counted as "different." The isotype of the sequences was also represented by colors following the color coding used in (C).

chronic model, the microglia lost their homeostatic ability (TGF-β) and phagocytic activity (Figure 7D). In addition, Aβ plaque intensity significantly increased, indicating that microglia can no longer prevent or control the growth of Aβ plaques. Therefore, we conclude that an increase in IgG can interfere with microglial function under conditions of excessive Aβ. We also speculated that the increase in B cells in AD is highly related to microglial dysfunction and dysregulation of Aβ clearance in microglia. This result corresponds to a previous report by Kim et al., which showed a therapeutic effect of B cell depletion (3xTg mice, AD mouse model versus 3xTg BKO, AD mouse model with B cell knock-out) through regulation of TGF-β^+ microglia in the brain (Kim et al., 2021). We also confirmed these results using transcriptome data deposited in the NCBI Gene Expression Omnibus (GEO) database (GEO: GSE165111) (Figure S14). The expression of TGF-β-related genes and TREM2 was significantly increased in 3xTg BKO mice, implying appropriate activation of microglial cells for phagocytosis (Keren-Shaul et al., 2017; Taylor et al., 2017). Moreover, GO analysis showed a significant increase in microglial responses (microglial cell activation, positive regulation of MCP1 production, positive microglial cell migration for biological processes, phagocytic vesicle membrane, phagocytic cup for cellular components, CCR chemokine receptor binding, cytokine activity, and CCR1 chemokine receptor

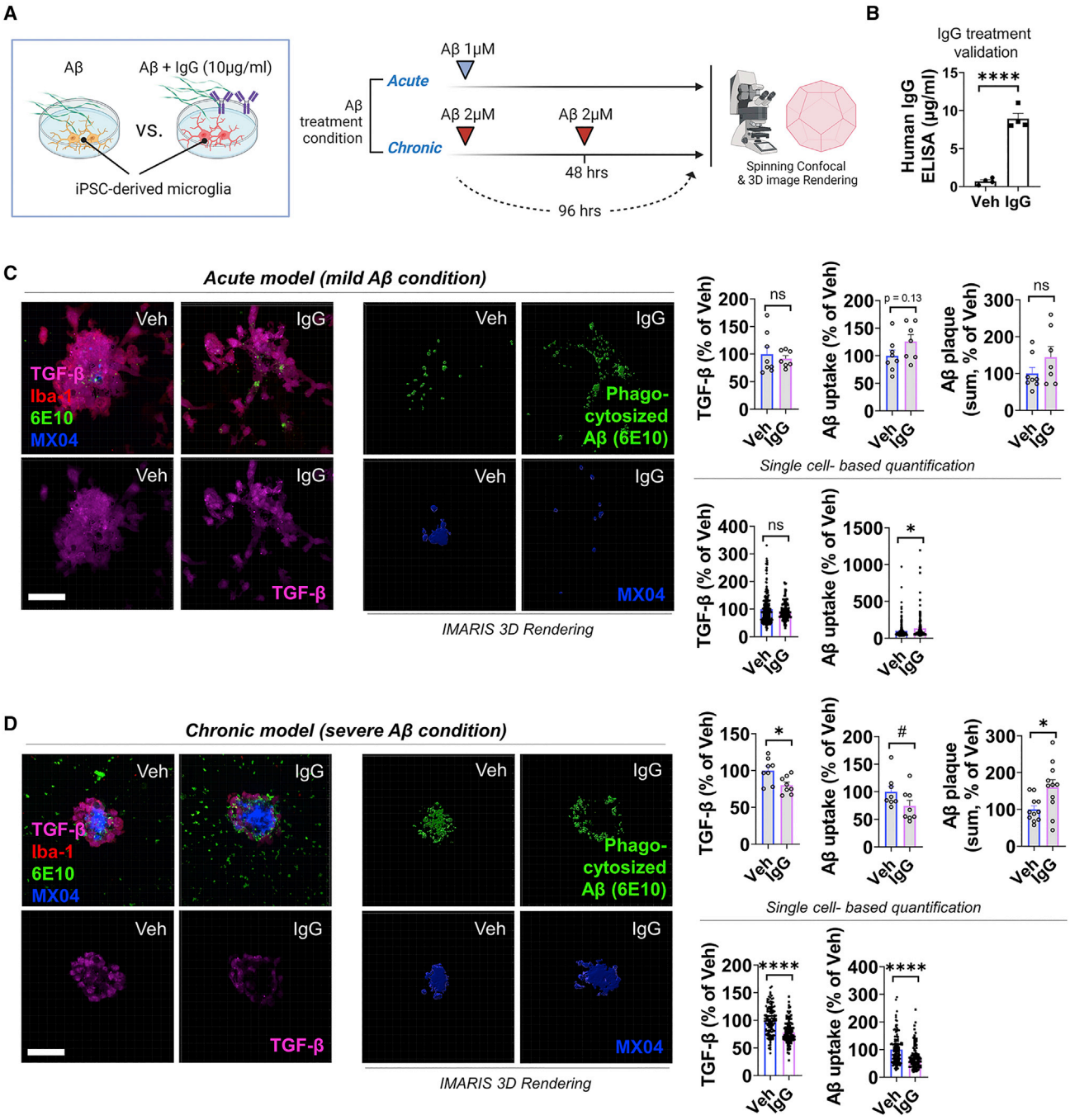

Figure 7. IgG can lead to the hyperactivation/chronic status of microglia and dysregulation of Aβ clearance

(A) A graphical summary of experimental conditions (acute versus chronic model).

(B) Validation of the levels of IgG in the conditioned media. ****$p < 0.0001$, independent t test ($n = 4$).

(C and D) Spinning disk confocal images and image (slice) or single-cell-based quantification of microglial TGF-β, phagocytosed beta-amyloid (Aβ), and Aβ plaque intensity both in acute and chronic models. For the quantification of phagocytosed Aβ and Aβ plaque, 3D rendering using IMARIS software was used. $^{\#}p < 0.1$, $^{**}p < 0.01$, $^{***}p < 0.001$, independent t test. For single cell-based quantification, each datapoint indicates individual microglial cells. Scale bar represents 40 μm. n = 7–8 slices (one to two Aβ plaques per one slice). Error bar, standard error of mean.

binding for molecular function) in 3xTg BKO mice. Thus, we speculate that therapeutic B cell depletion induces normal activation of microglial cells in the brain, whereas B cell increases in disease situations ultimately induces chronic/hypofunction of microglial cells and deposition of beta-amyloid plaques in the brain (Figure 7D). Figure S15 shows conjectured changes in

the B cell population, TGF-β, and microglial function with AD progression. Thus, we suggest that the immunological response of peripheral B lymphocytes is associated with neuropathology in the brains of AD patients.

DISCUSSION

This study investigated the association between B cells and their receptor repertoire in AD. We provide clear evidence for both quantitative and qualitative changes in B cells during the progression of AD. Although there have been several reports suggesting links between the population of B lymphocytes and the pathology of AD or clinical dementia symptoms, these studies relied on a cross-sectional study, and the results were controversial. For example, one prospective cohort study including 105 participants showed no differences in the percentage of B lymphocytes per total PBMC in patients with AD compared with that in healthy controls, but it identified an increased number of B lymphocytes producing autoantibodies against Aβ in AD (Sollvander et al., 2015). In contrast, other cross-sectional studies have found a decrease in B and T lymphocytes in patients with AD (Richartz-Salzburger et al., 2007; Tavolato and Argentiero, 1980; Tollefson et al., 1989). Although this discrepancy has been questioned continuously, many studies acknowledge the concept that lymphocytic abnormalities are accompanied by dementia, suggesting that the lymphocyte population could be a biomarker for AD (Rezai-Zadeh et al., 2009). A recent study identified the specific intracellular signaling marker, PLCγ2, in stimulated PBMC subsets from patients with AD through single-cell quantification and a machine learning model (Phongpreecha et al., 2020); however, the relevance of specific cell types among PBMC to AD pathology is still uncertain, especially in the B cell population. In the present study, our quantitative analyses revealed that the greater the increase is in the number of B lymphocytes, the greater is the brain Aβ deposition. The difference from previous studies is that we investigated the direct relationship with changes in brain Aβ through longitudinal analyses. We believe that this approach could lead to additional findings that would otherwise be difficult to identify in a cross-sectional study, and we revealed the longitudinal association between B lymphocytes and the pathology of AD.

Through our longitudinal study, we realized that it is worth closely monitoring the characteristics of B lymphocytes in patients with AD. Furthermore, since many of the latest technologies, such as unbiased next-generation TCR/BCR repertoire analysis or single-cell sequencing, have been developed, we thought it would be interesting to apply these technologies to our cohorts. Thus, we performed NGS-based BCR repertoire analysis for the deep profiling of BCR repertoire, and consequently, our analyses for B lymphocytes at the BCR sequence level identified the commonalities of BCR repertoires within AD patients implying the possibility of immunological stimuli by the common antigens such as plasma Aβ or tau proteins (Park et al., 2017; Park et al., 2019). Moreover, we could also speculate through the results from Figure 7 that changes in the B cell population and their secretion of IgG are related to brain microglial function regulating the expression of TGF-β in microglia (Li et al., 2017; Taylor et al., 2017). Since there is still debate that the decrease in the B cell population alleviates or exacerbates the deposition of Aβ (Kim et al., 2021; Xiong et al., 2021), our acute or chronic models for Aβ can partially explain this controversy in terms of microglial responses to IgG in the brain. In particular, our results correspond to those of Kim et al., who showed the therapeutic effect of B cell depletion through restoration of TGF-β in microglia (Kim et al., 2021).

Our approach through both longitudinal analysis and BCR repertoire profiling of AD suggests that the immunological response of peripheral B lymphocytes is clearly associated with neuropathology in the brain of patients with AD. Furthermore, the genetic information on BCR obtained from this study using next-generation repertoire analysis techniques can lead to the development of various immune-based therapeutics and treatments for AD.

Limitations of the study

Our work has some limitations, and we have provided suggestions for future study to overcome these.

First, we could not experimentally prove the relationship between BCR sequences exclusively shared among patients with AD and the disease state. We showed that AD-specific BCR sequences have distinctive patterns compared with the BCR sequences shared among patients with AD and normal individuals. We expect that the clonal information of AD-specific BCR sequences provided in this study can be utilized following additional validation.

Another concern is that we performed BCR repertoire analysis with only 13 participants. A validation study with a larger sample size is required to confirm these results.

STAR★METHODS

Detailed methods are provided in the online version of this paper and include the following:

- KEY RESOURCES TABLE
- RESOURCE AVAILABILITY
  - Lead contact
  - Materials availability
  - Data and code availability
- EXPERIMENTAL MODEL AND SUBJECT DETAILS
  - Study subjects
- METHOD DETAILS
  - Neuroimaging
  - Blood sampling and isolation and storage of peripheral blood mononuclear cells (PBMCs)
  - Flow cytometry
  - Preparation of next-generation sequencing (NGS) library
  - Consensus sequence extraction from raw NGS reads
  - Isotype annotation and functionality filtering of the consensus sequences
  - Divergence from germline V gene segments calculation
  - Removal of sequences subject to aerosol contamination
  - Pair-wise sharing analysis and inter-sample variable region full AA distance calculation

SUPPLEMENTAL INFORMATION

Supplemental information can be found online at https://doi.org/10.1016/j.celrep.2022.111391.

ACKNOWLEDGMENTS

We sincerely thank the subjects, staffs of hospitals, technical supporting team members, and volunteers for this project. The authors also appreciate the given ApoE4 isogenic iPSCs from Dr. Tsai at MIT. This work was supported by grants from the Ministry of Health and Welfare to I.M.-J. (HI19C1132020019, HU20C0187). This work was also supported by a grant of the KHIDI, funded by the Ministry of Health and Welfare (HI19C1339) and the National Research Foundation of Korea grant funded by the Korea government (MSIT) (NRF-2022R1C1C2012736) to J.-C.P. This work was supported by grants from the National Research Foundation of Korea to S.-H.H. (NRF2019R1I1A1A01063525). This work was also supported by the Global Research Development Center Program through the NRF funded by the Ministry of Science and ICT (MSIT) (2015K1A4A3047345), the Brain Korea 21 Plus Project in 2020, the Ministry of Science and ICT (MSIT) of the Republic of Korea, and the National Research Foundation of Korea (NRF-2020R1A3B3079653) to S.K. This work was also supported by Korea Initiative for fostering University of Research and Innovation Program of the National Research Foundation (NRF) funded by the Korean government (MSIT) (no. NRF-2020M3H1A1073304) to J.N. Graphical figures were created with BioRender.com, under J.-C.P.

AUTHOR CONTRIBUTIONS

J.-C.P., J.N., S.J., S.-H.H., S.K., and I.M.-J. conceptualized this study. J.-C.P., J.N., K.K., H.C., D.L., D.Y., and A.C.L. carried out the experiments. J.-C.P., J.N., S.J., H.L., and D.Y. analyzed the statistics. J.N., Y.L., and H.L. analyzed the NGS data. J.C. and D.Y.L. provided the resources. J.-C.P., J.N., S.J., and S.-H.H. wrote the original draft. S.K. and I.M.-J. reviewed and edited the manuscript.

DECLARATION OF INTERESTS

The authors declare no competing interests.

Received: February 28, 2022
Revised: July 4, 2022
Accepted: August 29, 2022
Published: September 20, 2022

REFERENCES

Allan, L.L., Hoefl, K., Zheng, D.J., Chung, B.K., Kozak, F.K., Tan, R., and van den Elzen, P. (2009). Apolipoprotein-mediated lipid antigen presentation in B cells provides a pathway for innate help by NKT cells. Blood *114*, 2411–2416. https://doi.org/10.1182/blood-2009-04-211417.

Baik, S.H., Kang, S., Lee, W., Choi, H., Chung, S., Kim, J.I., and Mook-Jung, I. (2019). A breakdown in metabolic reprogramming causes microglia dysfunction in Alzheimer's disease. Cell Metab. *30*, 493–507.e6. https://doi.org/10.1016/j.cmet.2019.06.005.

Bashford-Rogers, R.J.M., Bergamaschi, L., McKinney, E.F., Pombal, D.C., Mescia, F., Lee, J.C., Thomas, D.C., Flint, S.M., Kellam, P., Jayne, D.R.W., et al. (2019). Analysis of the B cell receptor repertoire in six immune-mediated diseases. Nature *574*, 122–126. https://doi.org/10.1038/s41586-019-1595-3.

Briney, B., Inderbitzin, A., Joyce, C., and Burton, D.R. (2019). Commonality despite exceptional diversity in the baseline human antibody repertoire. Nature *566*, 393–397. https://doi.org/10.1038/s41586-019-0879-y.

Byun, M.S., Yi, D., Lee, J.H., Choe, Y.M., Sohn, B.K., Lee, J.Y., Choi, H.J., Baek, H., Kim, Y.K., Lee, Y.S., et al. (2017). Korean brain aging study for the early diagnosis and prediction of Alzheimer's disease: methodology and baseline sample characteristics. Psychiatry Investig. *14*, 851–863. https://doi.org/10.4306/pi.2017.14.6.851.

Cao, W., and Zheng, H. (2018). Peripheral immune system in aging and Alzheimer's disease. Mol. Neurodegener. *13*, 51. https://doi.org/10.1186/s13024-018-0284-2.

Choe, Y.M., Sohn, B.K., Choi, H.J., Byun, M.S., Seo, E.H., Han, J.Y., Kim, Y.K., Yoon, E.J., Lee, J.M., Park, J., et al. (2014). Association of homocysteine with hippocampal volume independent of cerebral amyloid and vascular burden. Neurobiol. Aging *35*, 1519–1525. https://doi.org/10.1016/j.neurobiolaging.2014.01.013.

Cui, A., Di Niro, R., Vander Heiden, J.A., Briggs, A.W., Adams, K., Gilbert, T., O'Connor, K.C., Vigneault, F., Shlomchik, M.J., and Kleinstein, S.H. (2016). A model of somatic hypermutation targeting in mice based on high-throughput Ig sequencing data. J. Immunol. *197*, 3566–3574. https://doi.org/10.4049/jimmunol.1502263.

David Morgan, M., Richter, A., Al-Ali, S., Flint, J., Yiannakis, C., Drayson, M., Goldblatt, D., and Harper, L. (2016). Association of low B cell count and IgG levels with infection, and poor vaccine response with all-cause mortality in an immunosuppressed vasculitis population. Arthritis Care Res. *68*, 853–860. https://doi.org/10.1002/acr.22757.

Davis, C.W., Jackson, K.J.L., McElroy, A.K., Halfmann, P., Huang, J., Chennareddy, C., Piper, A.E., Leung, Y., Albariño, C.G., Crozier, I., et al. (2019). Longitudinal analysis of the human B cell response to ebola virus infection. Cell *177*, 1566–1582.e17. https://doi.org/10.1016/j.cell.2019.04.036.

de Bourcy, C.F.A., Angel, C.J.L., Vollmers, C., Dekker, C.L., Davis, M.M., and Quake, S.R. (2017). Phylogenetic analysis of the human antibody repertoire reveals quantitative signatures of immune senescence and aging. Proc. Natl. Acad. Sci. USA *114*, 1105–1110. https://doi.org/10.1073/pnas.1617959114.

Di Virgilio, M., Callen, E., Yamane, A., Zhang, W., Jankovic, M., Gitlin, A.D., Feldhahn, N., Resch, W., Oliveira, T.Y., Chait, B.T., et al. (2013). Rif1 prevents resection of DNA breaks and promotes immunoglobulin class switching. Science *339*, 711–715. https://doi.org/10.1126/science.1230624.

Ehrhardt, S.A., Zehner, M., Krähling, V., Cohen-Dvashi, H., Kreer, C., Elad, N., Gruell, H., Ercanoglu, M.S., Schommers, P., Gieselmann, L., et al. (2019). Polyclonal and convergent antibody response to Ebola virus vaccine rVSV-ZEBOV. Nat. Med. *25*, 1589–1600. https://doi.org/10.1038/s41591-019-0602-4.

Frasca, D., and Blomberg, B.B. (2009). Effects of aging on B cell function. Curr. Opin. Immunol. *21*, 425–430. https://doi.org/10.1016/j.coi.2009.06.001.

Frasca, D., and Blomberg, B.B. (2011). Aging affects human B cell responses. J. Clin. Immunol. *31*, 430–435. https://doi.org/10.1007/s10875-010-9501-7.

Frasca, D., and Blomberg, B.B. (2020). Aging induces B cell defects and decreased antibody responses to influenza infection and vaccination. Immun. Ageing *17*, 37. https://doi.org/10.1186/s12979-020-00210-z.

Gate, D., Saligrama, N., Leventhal, O., Yang, A.C., Unger, M.S., Middeldorp, J., Chen, K., Lehallier, B., Channappa, D., De Los Santos, M.B., et al. (2020). Clonally expanded CD8 T cells patrol the cerebrospinal fluid in Alzheimer's disease. Nature *577*, 399–404. https://doi.org/10.1038/s41586-019-1895-7.

Goldeck, D., Witkowski, J.M., Fülop, T., and Pawelec, G. (2016). Peripheral immune signatures in alzheimer disease. Curr. Alzheimer Res. *13*, 739–749. https://doi.org/10.2174/1567205013666160222112444.

Gupta, N.T., Adams, K.D., Briggs, A.W., Timberlake, S.C., Vigneault, F., and Kleinstein, S.H. (2017). Hierarchical clustering can identify B cell clones with high confidence in Ig repertoire sequencing data. J. Immunol. *198*, 2489–2499. https://doi.org/10.4049/jimmunol.1601850.

Han, S.H., Park, J.C., Byun, M.S., Yi, D., Lee, J.H., Lee, D.Y., and Mook-Jung, I.; KBASE Research Group (2019). Blood acetylcholinesterase level is a potential biomarker for the early detection of cerebral amyloid deposition in cognitively normal individuals. Neurobiol. Aging *73*, 21–29. https://doi.org/10.1016/j.neurobiolaging.2018.09.001.

Jack, C.R., Jr., Lowe, V.J., Senjem, M.L., Weigand, S.D., Kemp, B.J., Shiung, M.M., Knopman, D.S., Boeve, B.F., Klunk, W.E., Mathis, C.A., and Petersen, R.C. (2008). 11C PiB and structural MRI provide complementary information in imaging of Alzheimer's disease and amnestic mild cognitive impairment. Brain *131*, 665–680. https://doi.org/10.1093/brain/awm336.

Jackson, K.J.L., Liu, Y., Roskin, K.M., Glanville, J., Hoh, R.A., Seo, K., Marshall, E.L., Gurley, T.C., Moody, M.A., Haynes, B.F., et al. (2014). Human responses to influenza vaccination show seroconversion signatures and convergent antibody rearrangements. Cell Host Microbe *16*, 105–114. https://doi.org/10.1016/j.chom.2014.05.013.

Kasprowicz, D.J., Smallwood, P.S., Tyznik, A.J., and Ziegler, S.F. (2003). Scurfin (FoxP3) controls T-dependent immune responses in vivo through regulation of CD4+ T cell effector function. J. Immunol. *171*, 1216–1223. https://doi.org/10.4049/jimmunol.171.3.1216.

Keren-Shaul, H., Spinrad, A., Weiner, A., Matcovitch-Natan, O., Dvir-Szternfeld, R., Ulland, T.K., David, E., Baruch, K., Lara-Astaiso, D., Toth, B., et al. (2017). A unique microglia type Associated with restricting development of Alzheimer's disease. Cell *169*, 1276–1290.e17. https://doi.org/10.1016/j.cell.2017.05.018.

Kim, K., Wang, X., Ragonnaud, E., Bodogai, M., Illouz, T., DeLuca, M., McDevitt, R.A., Gusev, F., Okun, E., Rogaev, E., and Biragyn, A. (2021). Therapeutic B-cell depletion reverses progression of Alzheimer's disease. Nat. Commun. *12*, 2185. https://doi.org/10.1038/s41467-021-22479-4.

Klunk, W.E., Engler, H., Nordberg, A., Wang, Y., Blomqvist, G., Holt, D.P., Bergström, M., Savitcheva, I., Huang, G.F., Estrada, S., et al. (2004). Imaging brain amyloid in Alzheimer's disease with Pittsburgh Compound-B. Ann. Neurol. *55*, 306–319. https://doi.org/10.1002/ana.20009.

Lefranc, M.P. (2003). IMGT databases, web resources and tools for immunoglobulin and T cell receptor sequence analysis. Leukemia *17*, 260–266. https://doi.org/10.1038/sj.leu.2402637. http://imgt.cines.fr. Leukemia.

Li, Y., Shen, X.Z., Li, L., Zhao, T.V., Bernstein, K.E., Johnson, A.K., Lyden, P., Fang, J., and Shi, P. (2017). Brain transforming growth factor-beta resists hypertension via regulating microglial activation. Stroke *48*, 2557–2564. https://doi.org/10.1161/STROKEAHA.117.017370.

Lycke, N.Y., and Bemark, M. (2017). The regulation of gut mucosal IgA B-cell responses: recent developments. Mucosal Immunol. *10*, 1361–1374. https://doi.org/10.1038/mi.2017.62.

Parameswaran, P., Liu, Y., Roskin, K.M., Jackson, K.K.L., Dixit, V.P., Lee, J.Y., Artiles, K.L., Zompi, S., Vargas, M.J., Simen, B.B., et al. (2013). Convergent antibody signatures in human dengue. Cell Host Microbe *13*, 691–700. https://doi.org/10.1016/j.chom.2013.05.008.

Park, J.C., Barahona-Torres, N., Jang, S.Y., Mok, K.Y., Kim, H.J., Han, S.H., Cho, K.H., Zhou, X., Fu, A.K.Y., Ip, N.Y., et al. (2022). Multi-omics-based autophagy-related untypical subtypes in patients with cerebral amyloid pathology. Adv. Sci. *9*, e2201212. https://doi.org/10.1002/advs.202201212.

Park, J.C., Han, S.H., and Mook-Jung, I. (2020). Peripheral inflammatory biomarkers in Alzheimer's disease: a brief review. BMB Rep. *53*, 10–19.

Park, J.C., Han, S.H., Cho, H.J., Byun, M.S., Yi, D., Choe, Y.M., Kang, S., Jung, E.S., Won, S.J., Kim, E.H., et al. (2017). Chemically treated plasma Abeta is a potential blood-based biomarker for screening cerebral amyloid deposition. Alzheimer's Res. Ther. *9*, 20. https://doi.org/10.1186/s13195-017-0248-8.

Park, J.C., Han, S.H., Yi, D., Byun, M.S., Lee, J.H., Jang, S., Ko, K., Jeon, S.Y., Lee, Y.S., Kim, Y.K., et al. (2019). Plasma tau/amyloid-beta1-42 ratio predicts brain tau deposition and neurodegeneration in Alzheimer's disease. Brain *142*, 771–786. https://doi.org/10.1093/brain/awy347.

Phongpreecha, T., Fernandez, R., Mrdjen, D., Culos, A., Gajera, C.R., Wawro, A.M., Stanley, N., Gaudilliere, B., Poston, K.L., Aghaeepour, N., and Montine, T.J. (2020). Single-cell peripheral immunoprofiling of Alzheimer's and Parkinson's diseases. Sci. Adv. *6*, eabd5575. https://doi.org/10.1126/sciadv.abd5575.

Poinsatte, K., Smith, E.E., Torres, V.O., Ortega, S.B., Huebinger, R.M., Cullum, C.M., Monson, N.L., Zhang, R., and Stowe, A.M. (2019). T and B cell subsets differentially correlate with amyloid deposition and neurocognitive function in patients with amnestic mild cognitive impairment after one year of physical activity. Exerc. Immunol. Rev. *25*, 34–49.

Reiman, E.M., Chen, K., Liu, X., Bandy, D., Yu, M., Lee, W., Ayutyanont, N., Keppler, J., Reeder, S.A., Langbaum, J.B.S., et al. (2009). Fibrillar amyloid-beta burden in cognitively normal people at 3 levels of genetic risk for Alzheimer's disease. Proc. Natl. Acad. Sci. USA *106*, 6820–6825. https://doi.org/10.1073/pnas.0900345106.

Rezai-Zadeh, K., Gate, D., Szekely, C.A., and Town, T. (2009). Can peripheral leukocytes be used as Alzheimer's disease biomarkers? Expert Rev. Neurother. *9*, 1623–1633. https://doi.org/10.1586/ern.09.118.

Richartz-Salzburger, E., Batra, A., Stransky, E., Laske, C., Köhler, N., Bartels, M., Buchkremer, G., and Schott, K. (2007). Altered lymphocyte distribution in Alzheimer's disease. J. Psychiatr. Res. *41*, 174–178. https://doi.org/10.1016/j.jpsychires.2006.01.010.

Roth, D.B. (2014). V(D)J recombination: mechanism, errors, and fidelity. Microbiol. Spectr. *2*. https://doi.org/10.1128/microbiolspec.MDNA3-0041-2014.

Setliff, I., McDonnell, W.J., Raju, N., Bombardi, R.G., Murji, A.A., Scheepers, C., Ziki, R., Mynhardt, C., Shepherd, B.E., Mamchak, A.A., et al. (2018). Multi-donor longitudinal antibody repertoire sequencing reveals the existence of public antibody clonotypes in HIV-1 infection. Cell Host Microbe *23*, 845–854.e6. https://doi.org/10.1016/j.chom.2018.05.001.

Sievers, F., and Higgins, D.G. (2018). Clustal Omega for making accurate alignments of many protein sequences. Protein Sci. *27*, 135–145. https://doi.org/10.1002/pro.3290.

Sievers, F., Wilm, A., Dineen, D., Gibson, T.J., Karplus, K., Li, W., Lopez, R., McWilliam, H., Remmert, M., Söding, J., et al. (2011). Fast, scalable generation of high-quality protein multiple sequence alignments using Clustal Omega. Mol. Syst. Biol. *7*, 539. https://doi.org/10.1038/msb.2011.75.

Söllvander, S., Ekholm-Pettersson, F., Brundin, R.M., Westman, G., Kilander, L., Paulie, S., Lannfelt, L., and Sehlin, D. (2015). Increased number of plasma B cells producing autoantibodies against Abeta42 protofibrils in Alzheimer's disease. J. Alzheimers Dis. *48*, 63–72. https://doi.org/10.3233/JAD-150236.

Soto, C., Bombardi, R.G., Branchizio, A., Kose, N., Matta, P., Sevy, A.M., Sinkovits, R.S., Gilchuk, P., Finn, J.A., and Crowe, J.E., Jr. (2019). High frequency of shared clonotypes in human B cell receptor repertoires. Nature *566*, 398–402. https://doi.org/10.1038/s41586-019-0934-8.

Struemper, H., Kurtinecz, M., Edwards, L., Freimuth, W.W., Roth, D.A., and Stohl, W. (2022). Reductions in circulating B cell subsets and immunoglobulin G levels with long-term belimumab treatment in patients with SLE. Lupus Sci. Med. *9*, e000499. https://doi.org/10.1136/lupus-2021-000499.

Tavolato, B., and Argentiero, V. (1980). Immunological indices in presenile Alzheimer's disease. J. Neurol. Sci. *46*, 325–331. https://doi.org/10.1016/0022-510x(80)90057-x.

Taylor, R.A., Chang, C.F., Goods, B.A., Hammond, M.D., Mac Grory, B., Ai, Y., Steinschneider, A.F., Renfroe, S.C., Askenase, M.H., McCullough, L.D., et al. (2017). TGF-beta1 modulates microglial phenotype and promotes recovery after intracerebral hemorrhage. J. Clin. Invest. *127*, 280–292. https://doi.org/10.1172/JCI88647.

Tollefson, G.D., Godes, M., Warren, J.B., Haus, E., Luxenberg, M., and Garvey, M. (1989). Lymphopenia in primary degenerative dementia. J. Psychiatr. Res. *23*, 191–199. https://doi.org/10.1016/0022-3956(89)90024-1.

VanDyk, L., and Meek, K. (1992). Assembly of IgH CDR3: mechanism, regulation, and influence on antibody diversity. Int. Rev. Immunol. *8*, 123–133. https://doi.org/10.3109/08830189209055568.

Villaseñor, R., Ozmen, L., Messaddeq, N., Grüninger, F., Loetscher, H., Keller, A., Betsholtz, C., Freskgård, P.O., and Collin, L. (2016). Trafficking of endogenous immunoglobulins by endothelial cells at the blood-brain barrier. Sci. Rep. *6*, 25658. https://doi.org/10.1038/srep25658.

Vollmers, C., Sit, R.V., Weinstein, J.A., Dekker, C.L., and Quake, S.R. (2013). Genetic measurement of memory B-cell recall using antibody repertoire sequencing. Proc. Natl. Acad. Sci. USA *110*, 13463–13468. https://doi.org/10.1073/pnas.1312146110.

Weiss, S.J. (1989). Tissue destruction by neutrophils. N. Engl. J. Med. *320*, 365–376. https://doi.org/10.1056/NEJM198902093200606.

Xiong, L.L., Xue, L.L., Du, R.L., Niu, R.Z., Chen, L., Chen, J., Hu, Q., Tan, Y.X., Shang, H.F., Liu, J., et al. (2021). Single-cell RNA sequencing reveals B cell-related molecular biomarkers for Alzheimer's disease. Exp. Mol. Med. *53*, 1888–1901. https://doi.org/10.1038/s12276-021-00714-8.

Yaffe, K., Weston, A., Graff-Radford, N.R., Satterfield, S., Simonsick, E.M., Younkin, S.G., Younkin, L.H., Kuller, L., Ayonayon, H.N., Ding, J., and Harris, T.B. (2011). Association of plasma beta-amyloid level and cognitive reserve with subsequent cognitive decline. JAMA *305*, 261–266. https://doi.org/10.1001/jama.2010.1995.

Ye, J., Ma, N., Madden, T.L., and Ostell, J.M. (2013). IgBLAST: an immunoglobulin variable domain sequence analysis tool. Nucleic Acids Res. *41*, W34–W40. https://doi.org/10.1093/nar/gkt382.

STAR★METHODS

KEY RESOURCES TABLE

REAGENT or RESOURCE	SOURCE	IDENTIFIER
Antibodies		
FITC anti-human CD3 antibody	BioLegend	Cat# 317306; RRID: AB_571907
PE anti-human CD19 antibody	BioLegend	Cat# 302208; RRID: AB_314238
APC/Cy7 anti-human CD16 antibody	BioLegend	Cat# 302018; RRID: AB_314218
APC anti-human CD33 antibody	BioLegend	Cat# 303408; RRID: AB_314352
Anti-human TGF-beta antibody	Sigma Aldrich	Cat# SAB4502954; RRID: AB_10747473
Anti-6E10 antibody	Biolegend	Cat# 803001; RRID: AB_2564653
Anti-Iba1 antibody	SYSY	Cat# 234308; RRID: N/A
Biological samples		
Human peripheral blood mononuclear cells	This paper	N/A
Chemicals, peptides, and recombinant proteins		
DAPI reagent	Sigma Aldrich	D9542
Beta-amyloid 1–42	Bachem	H-8146
Methoxy-X04	This paper	N/A
Human IgG	ThermoFisher	02–7102
M-CSF	Peprotech	300–25
TGF-beta	Peprotech	100–21
IL-34	Peprotech	200–34
CX3CL1	Peprotech	300–31
CD200	Novoprotein	BP004
Deposited data		
PBMC RNA sequencing data	NCBI GEO2R	GEO: GSE18309 (https://www.ncbi.nlm.nih.gov/geo/query/acc.cgi?acc=GSE18309)
B cell-related RNA sequencing data	NCBI GEO2R	GEO: GSE165111 (https://www.ncbi.nlm.nih.gov/geo/query/acc.cgi?acc=GSE165111)
B cell Receptor Repertoire NGS Sequencing data	This study	BioProject: PRJNA667860 (https://www.ncbi.nlm.nih.gov/bioproject/?term=PRJNA667860)
Original codes	This study	GitHub: 1582538 (https://github.com/ad-bcr-repertoire/codes.git)
Experimental models: Cell lines		
Induced pluripotent stem cells (ApoE e4/e4 genotype)	Dr. Tsai at MIT	N/A
Software and algorithms		
R/R studio software	R Core Team	1.3.1056
Medcalc Software	MedCalc	20.111
GraphPad Prism 8	Dotmatics	8
Other		
Human TruStain FcX (Fc Receptor blocking solution)	BioLegend	422302
RPMI1640 media	Gibco	11875–093
FBS	Gibco	26140079
HBSS media	Welgene	LB003-02
FACS tube	BD Bioscience	352052
FACS tube strainer	BD Bioscience	352235
DMEM/F12 (no phenol red)	Gibco	11039021

RESOURCE AVAILABILITY

Lead contact

Further information and requests for resources and reagents should be directed to and will be fulfilled by the lead contact, Prof. Inhee Mook-Jung (Ph.D.), inhee@snu.ac.kr.

Materials availability

This study did not generate new unique reagents.

Data and code availability

- Publicly available transcriptome data are available in the NCBI GEO2R database. The sequencing data from this study are deposited in the NCBI BioProject database. The web links are listed in the key resources table.
- All original code has been deposited at GitHub and is publicly available as of the date of publication. The web link is listed in the key resources table.
- Any additional information required to reanalyze the data reported in this paper is available from the lead contact upon request.

EXPERIMENTAL MODEL AND SUBJECT DETAILS

Study subjects

A total of 133 participants were included and sorted into three groups for our longitudinal analysis: Pittsburgh compound B-positron emission tomography (PiB-PET; brain PET imaging for cerebral amyloid deposition) standardized uptake value ratio (SUVR) decrease group for two years (PiB^{Dec}, n = 33 including 14 males and 19 females; age, 73.97 ± 1.46), PiB stable group (PiB^{Stable}, n = 66 including 30 males 36 females; age, 67.51 ± 0.83), and PiB increase group (PiB^{Inc}, n = 34 including 15 males and 19 females; age, 72.79 ± 1.11) (Table S1). All subjects underwent brain imaging, namely structural MRI and PiB-PET, as well as psychological or clinical assessments, according to experts' guidelines. The assessments corresponded to neuropsychological tests based on the Korean Brain Aging Study for the Early diagnosis and prediction of AD (KBASE) protocol, along with Mini-Mental State Examination (MMSE) for neuropsychological assessment battery, which was performed in accordance with the Consortium to Establish a Registry for Alzheimer's Disease Assessment Packet (CERAD), and KBASE clinical assessment protocols (CERAD-K) (Byun et al., 2017). The MMSE z-score was calculated by the normalization of MMSE scores with appropriate correction for age, sex, and education levels. This study was approved under the recommendations of the Institutional Review Board (IRB) of the Seoul National University Hospital (SNUH), South Korea. Written informed consent was applied to all the participants, corresponding to the Declaration of Helsinki. Protocols and manuals were also approved by the IRB of the SNUH.

METHOD DETAILS

Neuroimaging

PiB-PET imaging and MR were conducted using a simultaneous 3.0 T PET-MR scanner (Biograph mMR Scanner; Siemens, Washington, D.C., USA), as previously described (Han et al., 2019). A total of 555 MBq of ^{11}C-PiB was injected intravenously, a PiB-PET emission scan was acquired, and the images were analyzed (Choe et al., 2014; Jack et al., 2008; Park et al., 2017; Reiman et al., 2009; Weiss, 1989). Prominent ^{11}C-PiB retention in the lateral temporal areas and brain regions has been described (Klunk et al., 2004), and regions of interest (ROIs) have been identified (Yaffe et al., 2011). The standardized uptake value ratio (SUVR) of each ROI was obtained by normalizing the mean value of all voxels in each ROI by the mean values of cerebellar uptake. Participants were divided into PiB-positive (PiB+) or PiB-negative (PiB-) based on the criteria of SUVR value of 1.4 in at least one of the four ROIs (Choe et al., 2014; Reiman et al., 2009).

Blood sampling and isolation and storage of peripheral blood mononuclear cells (PBMCs)

All blood samples were collected in the morning using K2 EDTA tubes (BD Vacutainer Systems, Plymouth, UK) following a period of overnight fasting. The EDTA tubes were immediately centrifuged and plasma supernatant was removed. The remaining blood was mixed with PBS and transferred into Ficoll-Hypaque solution for the isolation of PBMCs by establishing a gradient through repeated centrifugation and PBS washing cycles. The collected PBMCs were immediately cryopreserved using cell freezing buffer (90% fetal bovine serum +10% DMSO) and stored for one week in a Frosty Freezing Container (Thermo Scientific, Waltham, MA, USA). After a week, the vials were moved to an LN2 tank and stored at −192°C. Detailed information on the reagents used in this study is summarized in Table S2.

Flow cytometry

Cryopreserved PBMCs were recovered in RPMI 1640 media to be used for FACS flow cytometry analysis. After recovery, an HBSS-based FACS buffer containing 2% FBS and 0.05% sodium azide was used. For lymphocyte immunophenotyping, after excluding the pan-myeloid marker (CD33)-positive population, the remaining lymphocyte populations were identified as pan-T cell marker (CD3)-, pan-B cell marker (CD19)-, and pan-NK marker (CD16)-positive populations. Fluorescence-conjugated antibody information is

indicated in the text: APC anti-human CD33 antibody (1:100, clone WM53), FITC anti-human CD3 antibody (1:100, clone OKT3), PE anti-human CD19 antibody (1:100, clone HIB19), and APC/Cy7 anti-human CD16 antibody (1:100, clone Ts1/18). For immunostaining, cells were passed through a 35 μm nylon mesh strainer, blocked for 15 min on ice with Human TruStain FcX (5 μL/million cells in 100 μL staining volume, BioLegend), and stained for 30 min on ice with antibody mixture. DAPI staining (0.4 μg/mL) was performed to identify dead cells. Prepared cells were analyzed on a Fortessa X-20 (BD Biosciences), and the data were analyzed using FlowJo software (Tree Star). Detailed information on the reagents used in this study is summarized in Table S2.

Preparation of next-generation sequencing (NGS) library

Cryopreserved $CD19^+$ B lymphocytes were thawed, and total RNA samples were extracted using the TRIzol Plus RNA Purification Kit, developed by Life Technologies Company. One microgram of total RNA was used as the input volume for library preparation. Next, reverse transcription was conducted according to the manufacturer's guideline using SuperScript IV reverse transcriptase (Life Technologies) and primers for five immunoglobulin heavy chain isotypes containing UMI (unique molecular identifiers) barcodes that consist of 14 random nucleotides and partial Illumina adapters (Table S3). Primer annealing was performed at 72°C for 3 min, and then immediately placed on ice for 2 min. First-strand cDNA was purified using AmPure XP beads (Beckman Coulter) at a 1:1.8 ratio and second-strand cDNA was synthesized using KAPA HiFi HotStart DNA polymerase (Kappa Bioscience) and a pool of six immunoglobulin heavy chain variable region-specific primers (Table S5; 98°C for 4 min, 52°C for 1 min, and 72°C for 5 min) (Briney et al., 2019; Vollmers et al., 2013). Double-stranded cDNA was purified via AmPure XP beads (Beckman Coulter) at a 1:1 ratio. After that, it was amplified using KAPA HiFi HotStart DNA polymerase (Kappa Bioscience) using double primers consisting of Illumina adapters and index sequences (95°C for 3 min, 25 cycles of 95°C for 30 s, 65°C for 30 s, 72°C for 1 min, and 72°C for 5 min). The final NGS libraries were obtained using AmPure XP beads (Beckman Coulter) at a 1:1 ratio and were subjected to QC on TapeStation 2200 (Agilent Technologies). Libraries with a single peak of correct sequence length were assigned to NGS analysis using the Illumina sequencing platforms MiSeq, for AD and Normal datasets, and NovaSeq for Normal2 dataset.

Consensus sequence extraction from raw NGS reads

The raw NGS reads were q-filtered using the q20p95 condition, which means that 95% of the reads needed to have Phred scores higher than 20. On average, 83.51% of the reads passed the q-filtering condition. The primer regions used in the experiments were then extracted from the reads while allowing for one mismatch (substitution, insertion, or deletion). Based on the location of the primer sequences, the UMI sequences were extracted, and the reads were clustered according to the UMI sequences. The reads in the same UMI clusters were aligned using the multiple sequence alignment tool Clustal Omega 1.2.4 (Sievers and Higgins, 2018; Sievers et al., 2011). The consensus sequences of the UMI clusters were extracted using the nucleotide frequency information of the alignment results, and the read count of the sequences was re-defined as the number of unique UMI sequences.

Isotype annotation and functionality filtering of the consensus sequences

The constant region of the consensus sequences was used for isotype annotation. The constant region sequences were recognized in a location-based manner, and then the sequences were aligned to an in-house constant gene database constructed based on the IMGT (the international immunogenetics information system) database (Lefranc, 2003). The isotypes of the consensus sequences were determined using alignment results. The V/D/J genes and CDR1/2/3 regions of the sequences were then extracted and annotated using IgBLAST 1.8.0 (Ye et al., 2013). After annotation, non-functional consensus sequences were filtered out using the following conditions: 1. Sequence length is less than 250 bp 2. The existence of a stop codon or a frameshift in complete AA sequences and 3. Annotation failure is more than or equal to that of the CDR1/2/3 regions.

Divergence from germline V gene segments calculation

As the first step in the divergence calculation, the B-cell-receptor (BCR) sequences were aligned to germline variable gene segments using IgBLAST (Ye et al., 2013). Based on the IgBLAST alignment results, the lengths of the sequences aligned to the gene segments and the number of mutations within the aligned region were calculated. We defined the divergence value as the number of mutations divided by the aligned length, as previously described (Soto et al., 2019).

Removal of sequences subject to aerosol contamination

We conducted a sharing analysis to define the AD-specific group among the whole BCR sequences of each repertoire. Identical BCR sequences derived from experimental faults or aerosol contamination may contribute to the occurrence of false high sharing between the BCR repertoires. Thus, to mitigate the effect of such errors, we removed the BCR sequences that have fully identical nucleotides, including the UMI region, from other BCR repertoires. This is based on the fact that the possibility of two fully identical nucleotide sequences being detected in different repertoires is very low, considering the complexity of UMI design and the natural diversity of BCR repertoires.

Pair-wise sharing analysis and inter-sample variable region full AA distance calculation

Pairwise sharing analysis was conducted at the BCR lineage level. A previously reported hierarchical clustering method was used (Gupta et al., 2017). BCR lineages satisfying the following conditions from two different repertoire data sets were merged and defined as shared

BCR lineages: (1) The V/J gene usage, (2) the same CDR3 sequence length, and (3) CDR3 AA sequence homology being more than 0.7. In the above condition, CDR3 AA sequence homology was set as one minus CDR3 AA sequence discrepancy, which was calculated by the minimum Hamming distance in the CDR3 AA sequence between all combinations of BCR sequences from two different BCR lineages divided by CDR3 AA sequence length. The BCR sequences of the shared BCR lineages were defined as shared BCR sequences. To define the inter-sample variable region full AA distance, BCR sequences from the same shared BCR lineages were used. First, the variable region full AA sequence of the BCR sequences in the same shared BCR lineages was trimmed and aligned. The Hamming distance in the variable-region full AA sequence between all combinations of BCR sequences from two different samples was then calculated. Among the calculated Hamming distance values, the minimum value was set as the inter-sample variable region full AA distance value of the shared BCR lineage.

RNA sequencing analysis

The public transcriptome data in the GEO2R public database (accession number: GEO: GSE18309 and GEO: GSE165111 with the following available link for Figures 4 and S14: https://www.ncbi.nlm.nih.gov/geo/query/acc.cgi?acc=GSE18309 and https://www.ncbi.nlm.nih.gov/geo/query/acc.cgi?acc=GSE165111) was used for RNA sequencing analysis. All analyses were performed using a GEO2R analyzer. To obtain B cell-related targets, we adopted the Gene Ontology (GO) database Amigo2 (http://amigo.geneontology.org/) and sorted the B cell-related genes. Genes that significantly overlapped with the Amigo2 database were used for Figure 4. To perform GO analysis using differentially expressed genes (DEGs) from GSE165111, the Database for Annotation, Visualization, and Integrated Discovery (DAVID) bioinformatics resources were used.

Randomized sharing simulation

To calculate the statistical significance of the shared Ig count values, we conducted a randomized sharing simulation using the Normal2 NGS data (Figure 6B). First, all processed NGS data was subsampled to meet the throughput threshold of 250,000 reads. For NGS data lacking the throughput for sub-sampling, all the sequences in the data were subjected to the following analysis: after selecting 10 subjects randomly from the Normal2 dataset, highly similar BCRs were defined in a pairwise manner, as in the case of AD&AD (Tables S3 and S4). This analysis was conducted 100,000 times to cover as many combinations as possible in the Normal2 dataset. Then, the shared Ig count values were drawn in a histogram, and we counted the number of cases where the Ig count was more extreme than the observed shared Ig counts in AD&AD. The number of extreme cases divided by 100,000 was used to define the p *value* of the shared Ig counts in AD&AD.

Induced pluripotent stem cell (iPSC)-derived microglial cell culture, IgG treatment, and imaging

iPSC-derived microglia were generated according to the protocol described in our previous study (Park et al., 2022). Monomeric Aβ 1–42 (1 μM; Bachem Holding, Bubendorf, Switzerland) was used for 4 days to mimic mild Aβ (acute model) conditions. For severe Aβ (chronic model) conditions, monomeric Aβ (2 μM) was administered for 4 days, with an additional shock using monomeric Aβ (2 μM) on day 2. Human IgG (10 μg/mL; ThermoFisher Scientific, Massachusetts, United States) was also added for 4 days to mimic the increase in B cell population or IgG counts. To capture images of microglia, we used a spinning disc confocal microscope (Yokogawa, CSU-X1; Tokyo, Japan). To quantify intracellular TGF-β, intracellular beta-amyloid, and Aβ plaque intensity, 3D rendering and masking processes were performed using the IMARIS software (Bitplane, Zurich, Switzerland). Methoxy-X04 (MX04) solution (10% MX04, 45% propylene glycol and 45% PBS) was used to stain Aβ plaques. The antibodies used are listed in STAR Methods.

QUANTIFICATION AND STATISTICAL ANALYSIS

All statistical analyses were performed using GraphPad Prism 8 (San Diego, CA, USA), or MedCalc software (Acacialaan, Ostend, Belgium) when appropriate. Categorical data was analyzed using the chi-square test. Independent *t*-test and ANOVA post-hoc tests were used to compare numerical data. Outliers were excluded using Grubb's test. The association between the values was determined using partial correlation analyses, with correction for several covariates. A multiple regression analysis was also performed. To test the discriminatory power of the variables, logistic regression followed by receiver operating characteristic (ROC) curve analysis, and precision-recall curve analysis, with the bootstrap method (1000 iterations, random number seed = 978) to mimic the randomized sampling process, were conducted. To compare the numerical values used in the pairwise sharing analysis, the Wilcoxon rank-sum test was conducted after the Shapiro–Wilk test.

ADDITIONAL RESOURCES

Not applicable.

Ethical approval

This study was approved under the recommendations of the Institutional Review Board (IRB) of the Seoul National University Hospital (SNUH), South Korea. Written informed consent was applied to all the participants, corresponding to the Declaration of Helsinki. Protocols and manuals were also approved by the IRB of the SNUH.